Analytica Chimica Acta 1210 (2022) 339883

Contents lists available at ScienceDirect

Analytica Chimica Acta

journal homepage: www.elsevier.com/locate/aca

# Quenching of tungsten-based polyoxometalate nanoclusters on electrochemiluminescence emission of luminol loaded $CeVO_4$/Au for immunoassay of protein

Yu Du [a,b], Siqi Yu [a], Huangxian Ju [a,*]

[a] State Key Laboratory of Analytical Chemistry for Life Science, School of Chemistry and Chemical Engineering, Nanjing University, Nanjing, 210023, China
[b] Collaborative Innovation Center for Green Chemical Manufacturing and Accurate Detection, University of Jinan, Jinan, 250022, China

## HIGHLIGHTS

- An ECL immunosensing method is proposed using tungsten-based quencher as signal tag.
- The tag can efficiently quench the ECL emission of Lu-$CeVO_4$/Au/$H_2O_2$ via the consumption of $O_2$.$^{\bullet-}$.
- This immunoassay method for NSE shows good operability and high sensitivity with a LOD of 0.19 pg/mL.
- The quenching effect offers an effective tag for immunoassay of protein biomarkers.

## GRAPHICAL ABSTRACT

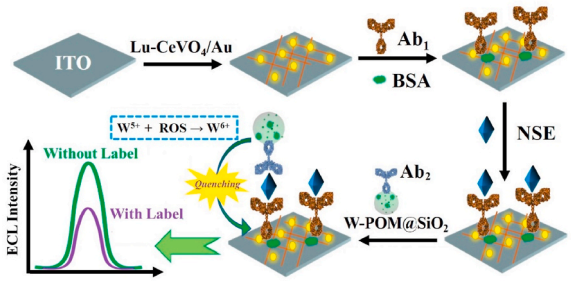


## ARTICLE INFO

*Keywords:*
Electrochemiluminescence
Immunosensor
Polyoxometalate nanocluster
Luminol
Neuron-specific enolase
Immunoassay

## ABSTRACT

A quenching-typed electrochemiluminescence (ECL) immunosensing method was proposed for protein detection by the redox reaction of tungsten-based polyoxometalate nanoclusters (W-POM NCs) with free radical ($O_2^{\bullet-}$) as the intermediate of co-reactant $H_2O_2$. The immunosensor was constructed by co-immobilizing luminol loaded $CeVO_4$/Au nanohybrids and capture antibody on an indium tin oxide electrode, which showed strong ECL emission in the presence of $H_2O_2$ due to the catalysis of $CeVO_4$/Au toward its electro-oxidation to produce $O_2^{\bullet-}$ via the reversible conversion between $Ce^{3+}$ and $Ce^{4+}$. The W-POM NCs were encapsulated in the uniformly sized amino-silica nanosphere ($SiO_2$) to act as a label (W-POM@$SiO_2$) of the secondary antibody. Upon the sandwich-typed immunoreactions with the target, the W-POM NCs were introduced onto the immunosensor surface to reduce $O_2^{\bullet-}$, and thus quenched the ECL emission of luminol-$H_2O_2$ system. Using neuron-specific enolase (NSE) as a target, the proposed method showed a detection limit of 0.19 pg/mL and detectable range of 0.5 pg/mL to 18 ng/mL. The excellent performance of the proposed "ON-OFF" strategy demonstrated that the W-based quenching offers an effective tag for immunoassay of protein biomarkers.

* Corresponding author.
*E-mail address:* hxju@nju.edu.cn (H. Ju).

https://doi.org/10.1016/j.aca.2022.339883
Received 13 March 2022; Received in revised form 23 April 2022; Accepted 27 April 2022
Available online 29 April 2022

## 1. Introduction

Electrochemiluminescence (ECL) as a promising analytical technology owns superiorities of high sensitivity, low background, precise temporal and spatial control on light emission process with assistance of electrochemical technique [1–3]. ECL quenching effect based on resonance energy transfer (RET) has been demonstrated as an effective approach for improving the performance of biosensing methods [4,5]. RET-based ECL quenching mechanism is attractive, but it has exact demand on the nano-distance between donors and acceptors while the area size of effective spectral overlap is hard to control [6]. Alternatively, charge transfer-based quenching mechanism has been reported using the fabulous $Ru(bpy)_3^{2+}$-TPrA system as model, in which ferrocene (Fc) is selected as a quencher to consume the excited $Ru(bpy)_3^{2+}$ via a charge-transfer involved redox reaction, leading to efficient suppression on ECL emission without exact demands [7]. However, direct consumption of produced excited luminophores somehow accelerates the ECL reaction between reduced or oxidized luminophore molecule and intermediate free radical of coreactant, which produces more excited molecules for ECL emission, thus affecting the quenching efficiency during the sensing process.

As one of the most widely used ECL reagents, luminol has drawn considerable attention due to the high luminous efficiency, nontoxicity, and low excitation potential. The related ECL emission involves the presence of superoxide radical ($O_2^{\bullet-}$) produced from the electro-oxidation of $H_2O_2$ [8]. By employing different nanomaterials to design efficient sensing strategies, the ECL behavior of luminol can be dramatically improved [9–12]. Some mixed-valence cerium-doped nanomaterials have been used to fabricate the electrochemical sensing devices due to their excellent electrocatalytic activities [13,14]. For example, $CeO_2/SnS_2$ heterostructure can be used as an efficient coreaction accelerator for the generation of superoxide anions of $O_2^{\bullet-}$ and thus the improvement of the detection sensitivity [15], and $CeVO_4$ nanomaterials have been demonstrated to display the satisfying intrinsic peroxidase-mimic activity for $H_2O_2$ detection since Ce element can reversibly convert between $Ce^{3+}$ and $Ce^{4+}$ [14]. In view of this promising biomimetic properties, this work fabricated a $CeVO_4$ nanoarray with large specific surface area to construct a new biomimetic ECL sensing platform of luminol-$H_2O_2$ system by immobilizing luminol loaded $CeVO_4$/Au nanohybrids (Lu-$CeVO_4$/Au) on an indium tin oxide (ITO) electrode. The accelerated ECL reaction between luminol and $H_2O_2$ in a catalytic manner led to a strong ECL emission.

To make use of the strong ECL emission for immunoassay, a quenching system was designed by labeling the secondary antibody ($Ab_2$) with tungsten-based polyoxometalate nanoclusters (W-POM NCs). Polyoxometalates (POMs) are a kind of early transition metal oxygen anion clusters with well-defined structure and distinct sizes, and have revealed widespread applications in catalysis [16], material science [17], medicine [18], macromolecular crystallography [19] and so on. Among all of the POMs, the stable and biocompatible W-POM NCs have received much attention due to the existence of W element with mixed valence states of $W^{5+}$ and $W^{6+}$. The reductive $W^{5+}$ in W-POM NCs can be oxidized to $W^{6+}$ by reactive oxygen species (ROSs), thus performing excellent ROSs-scavenging activity [20–23]. Here the redox reaction between W-POM NCs and $O_2^{\bullet-}$ radicals, the electro-oxidation intermediate of $H_2O_2$ in ECL process, resulted in an "Off-On" ECL signal switch. Using neuron-specific enolase (NSE), a distinctly important reference marker for accurate diagnosis of small cell lung cancer (SCLC) in early stage [24], as a target, the immunoassay could be performed by co-immobilizing its capture antibody ($Ab_1$) on the Lu-$CeVO_4$/Au modified ITO electrode and labeling W-POM NCs to its $Ab_2$ (Scheme 1). The efficient ECL quenching upon the sandwich-typed immunoreactions with NSE produced a sensitive immunosensing method for NSE detection. The wide detectable range with a detection limit of 0.19 pg/mL demonstrated the potential application of the proposed W-based quenching system in the detection of protein biomarkers.

## 2. Experimental

### 2.1. Reagents and materials

$Ab_1$ and $Ab_2$ against NSE were obtained from Biosynthesis Biotechnology Co., Ltd., (Beijing, China). $Ce(NO_3)_3{\cdot}6H_2O$, ethylene diamine tetraacetic acid (EDTA), $Na_3VO_4$ and $HAuCl_4$ were purchased from shanghai Macklin Biochemical Co. Ltd. (Shanghai, China). Bovine serum albumin (BSA) (96%–99%) was purchased from Aladdin Industrial Corporation (Shanghai, China). All other chemicals were of analytical reagent grade and were used without further purification. Phosphate buffered solution (PBS) was prepared using 1/15 M $Na_2HPO_4$ and 1/15 M $KH_2PO_4$ solution. 2.5 mM $K_3Fe(CN)_6/K_4Fe(CN)_6$ and 0.1 M $KNO_3$ solution were used as electrolyte to obtain electrochemical impedance spectra (EIS). Ultrapure water (18.25 MΩ cm, 24 °C) was used for all the experiments.

### 2.2. Apparatus

X-ray photoelectron spectra (XPS) was acquired with Thermo ESCALAB 250XI (America). Scanning electron microscopic images (SEM) were recorded on JEOL JSM-6700F microscope (Japan). XRD patterns of the prepared samples were acquired with a Rigaku D/MAX 2200 X-ray diffractometer (Tokyo, Japan) using CuKα radiation (40 kV, 300 mA) of wavelength 0.154 nm to confirm the structure of the

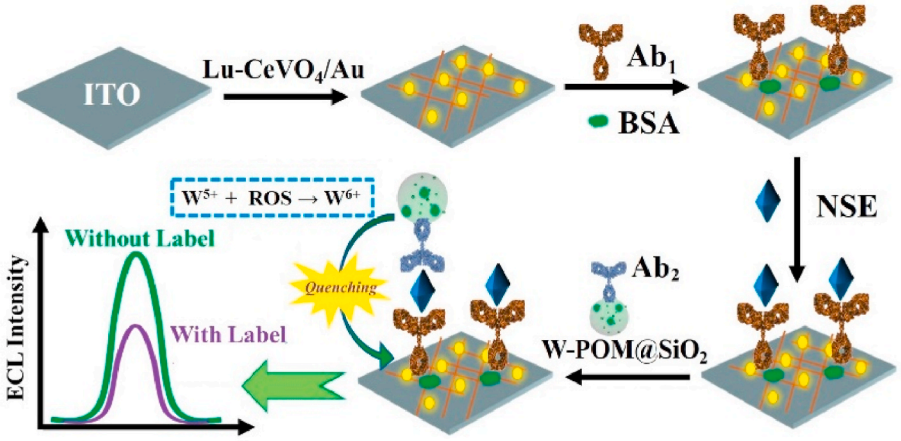


**Scheme 1.** Schematic illustration for label quenched ECL immunosensing.

materials. The UV–vis absorbance spectra were detected with a TU-1901 UV–vis Spectrophotometer (Beijing Purkinje General instrument co. Ltd, China). ECL measurements were performed with MPI-F flow-injection chemiluminescence detector (Xi'an remax Electronic Science Tech. Co. Ltd., China), and electrochemical measurements were carried out on CHI760D electrochemical workstation (Chenhua Instrument Shanghai Co., Ltd, China).

### 2.3. Preparation of Lu-$CeVO_4$/Au nanohybrids

$CeVO_4$ nanorod arrays (NAs) were synthesized by a reported method [25]. Briefly, 434.1 mg $Ce(NO_3)_3{\cdot}6H_2O$ and 292.2 mg EDTA were added into 15 mL ultrapure water with stirring 15 min. Afterward, 15 mL $Na_3VO_4$ solution containing 183.9 mg $Na_3VO_4$ was added in the mixture. After stirring 20 min, the pH of the mixture was adjusted to 9 by adding $NH_3{\cdot}H_2O$ dropwise. Subsequently, this mixture was placed into an autoclave at 180 °C for 18 h. The resulting product ($CeVO_4$ NAs) was centrifuged and washed for three times, and finally dried at 60 °C in vacuum.

Next, 20 mg $CeVO_4$ NAs were dispersed in 30 mL ultrapure water with ultrasonication for 1 h, followed by the sequent addition of 1 mL of $HAuCl_4$ (1 wt%) and 5 mg polyvinylpyrrolidone (PVP). After stirring for 6 h, 2 mL 50 mM sodium citrate and a bit of $NaBH_4$ were added dropwise to reduce $HAuCl_4$. After stirring for 12 h, the $CeVO_4$/Au nanohybrids were obtained by washing the mixture with ultrapure water to remove unbonded Au nanoparticles.

Finally, the obtained $CeVO_4$/Au nanohybrids were redispersed in 5 mL ultrapure water. 1 mL 5 mM luminol (pH 7.4) was then mixed under oscillating for 12 h, during which luminol could be loaded on $CeVO_4$/Au nanohybrids via covalent linkage between Au and the amino-of luminol. After centrifuging to remove dissociative luminol, the Lu-$CeVO_4$/Au nanohybrids were dried in vacuum at 35 °C, and dispersed in 0.5% chitosan solution.

### 2.4. Preparation of $Ab_2$-W-POM@$SiO_2$

W-POMs were prepared by slight modification of the previously reported synthetic method [20]. Firstly, 100 mg gallic acid was dispersed in 6 mL ultrapure water. After completely dissolved, 1.0 mL of 60 mg/mL $H_3O_{40}PW_{12}{\cdot}xH_2O$ was added into the solution with stirring intensely for 5 min. Subsequently, 3.0 mL $Na_2CO_3$ solution (7.5 w%) was injected into the solution to obtain a dark green solution with continuous stirring for 5.0 h. Then this solution was purified for 3 days through dialysis method (dialysis bag, Mw = 3500 Da) to remove any unreacted raw reagent. Afterward, a lyophilization process was used to dry W-POMs, which were stored at 4 °C.

The W-POM@$SiO_2$ was synthesized by adding W-POMs during the preparing process of $SiO_2$ nanosphere. Briefly, 15 mg W-POM power was dispersed in 1.5 mL of ultrapure water. Afterward, 2 mL of absolute ethyl alcohol was added in the W-POM dispersion and stirred for 5 min. Then, 100 μL of TEOS and 200 μL of $NH_3{\cdot}H_2O$ were injected quickly and in turn into the solution to stir for 12 h. The final product of W-POM@$SiO_2$ was collected by centrifugation, and refluxed with alcoholic APTES solution for 24 h at 125 °C to finish amino-functionalization. After removing the unbound APTES by centrifugation, the amino-functionalized W-POM@$SiO_2$ was dispersed in pH 7.4 PBS.

Lastly, $Ab_2$-W-POM@$SiO_2$ was prepared by adding 500 μL of $Ab_2$ (100 μg/mL) in the obtained W-POM@$SiO_2$ solution with the assistance of 1 mL of freshly prepared 400 mM EDC and 100 mM NHS mixture. After continuously stirred for 24 h at 4 °C, the excessive EDC, NHS, and $Ab_2$ molecules were discarded by centrifugation. The resulting $Ab_2$-W-POM@$SiO_2$ were dispersed in pH 7.4 PBS and stored at 4 °C.

### 2.5. Fabrication of immunosensor

The immunosensor was prepared using an ITO chip with area of 1 × 1.5 $cm^2$ as shown in Scheme 1. After drying the clean chip at 70 °C, 6 μL of 5 mg/mL Lu-$CeVO_4$/Au was cast on its surface. Subsequently, 6 μL of $Ab_1$ (50 μg/mL) was dropped on Lu-$CeVO_4$/Au substrate and incubated at 4 °C overnight to immobilize $Ab_1$ through the interaction of AuNPs with amino group of antibody. After thoroughly rinsing with ultrapure water to remove unbound $Ab_1$ and drying at 4 °C, 3 μL of BSA (*wt.*0.1%) was further used to block the left non-specific active sites. After removing the useless BSA by rinsing, the immunosensor was obtained for ECL measurements.

### 2.6. ECL measurements

After the samples containing NSE with different concentrations were incubated on the immunosensors for 2 h at 37 °C, 6 μL of $Ab_2$-W-POM@$SiO_2$ solution was dropped on the surface to incubate for 2 h at 37 °C. The ECL measurements were performed by potential steps between 0 (10 s) and 0.6 V (1 s) in 1/15 M PBS (pH 8.0) containing 8 mM $H_2O_2$ using the formed ITO/Lu-$CeVO_4$/Au/$Ab_1$(BSA)/NSE/$Ab_2$-W-POM@$SiO_2$, a platinum electrode and a saturated Ag/AgCl electrode as the working, counter and reference electrodes, respectively. The photomultiplier tube (PMT) was set at 650 V.

## 3. Results and discussion

### 3.1. Characterization of different nanomaterials

The $CeVO_4$ NRs were hydrothermally prepared in salty solution with assistance of a multidentate ligand of EDTA. The size and morphology of the obtained NRs were ascertained using SEM (Fig. 1A), which revealed a homogeneous dispersion of nanorod nanostructure with an average length of 200 nm and width of 10 nm. The structure and crystallinity of $CeVO_4$ NRs were determined by X-ray powder diffraction (XRD) pattern, which showed the same diffraction peaks as pure tetragonal (zircon-type) $CeVO_4$ phase (JCPDS No-12-0757) without impurity peak (Fig. 1B), confirming the pure phase of the prepared $CeVO_4$ NRs. In particular, the diffraction peaks appeared at the 2θ values of 18.1°, 24°, 32.4° and 47.9° could be indexed to the crystal planes (101), (200), (112) and (312), respectively. The survey of XPS spectrum of $CeVO_4$ NRs successfully confirmed the existence of Ce 3d, V 2p, O 1s and C 1s (Fig. 1C). The high-resolution spectrum of Ce 3d exhibited two characteristic peaks belonging to Ce $3d_{5/2}$ orbital at about 885.1 and 881.2 eV, and the peaks belonging to Ce $3d_{3/2}$ orbital at about 903.3 and 899.6 eV (Fig. 1D), implying the existence of $Ce^{3+}$ ions with an identical +3 valence state. Besides, the V 2p spectrum showed two peaks at 515.8 eV and 523.5 eV (Fig. 1E), which were separately ascribed to V $2p_{3/2}$ and V $2p_{1/2}$, and proved an identical +5 valence state for V element. The high-resolution XPS spectrum of O 1s showed two peaks at 528.8 eV and 530.4 eV (Fig. S1), which might indicate two species of lattice oxygen ($O_2$) in $CeVO_4$ NRs. The morphology of $CeVO_4$/Au NRs indicated the successful in situ growth of large amount of Au NPs on $CeVO_4$ NRs (Fig. 1F), which was further confirmed by the presence of elements Ce, O, V, and Au in the EDX of $CeVO_4$/Au NRs (Fig. 1G).

The morphology of W-POM@$SiO_2$ was characterized as shown in Fig. 2A, which displayed smooth sphere without crack and the particle size of about 500 nm. The scanning elemental mapping of W-POM@$SiO_2$ indicated the existence of Si, O and W (Fig. 2B–D), confirming that W-POMs were successfully doped in $SiO_2$ nanospheres.

### 3.2. Quenching mechanism of W-POM@$SiO_2$ on ECL of luminol-$H_2O_2$ system

Under continuous potential steps between −0.6 V and 0.6 V, the Lu-$CeVO_4$/Au modified ITO showed obvious oxidation current and ECL signal in pH 8.0 PBS containing 6 μM $H_2O_2$ (Fig. 3A, curves a and b), which could be ascribed to the responses of Lu-$CeVO_4$/Au/$H_2O_2$ system. Moreover, the ECL signal was very stable (Fig. 3B). The strong responses

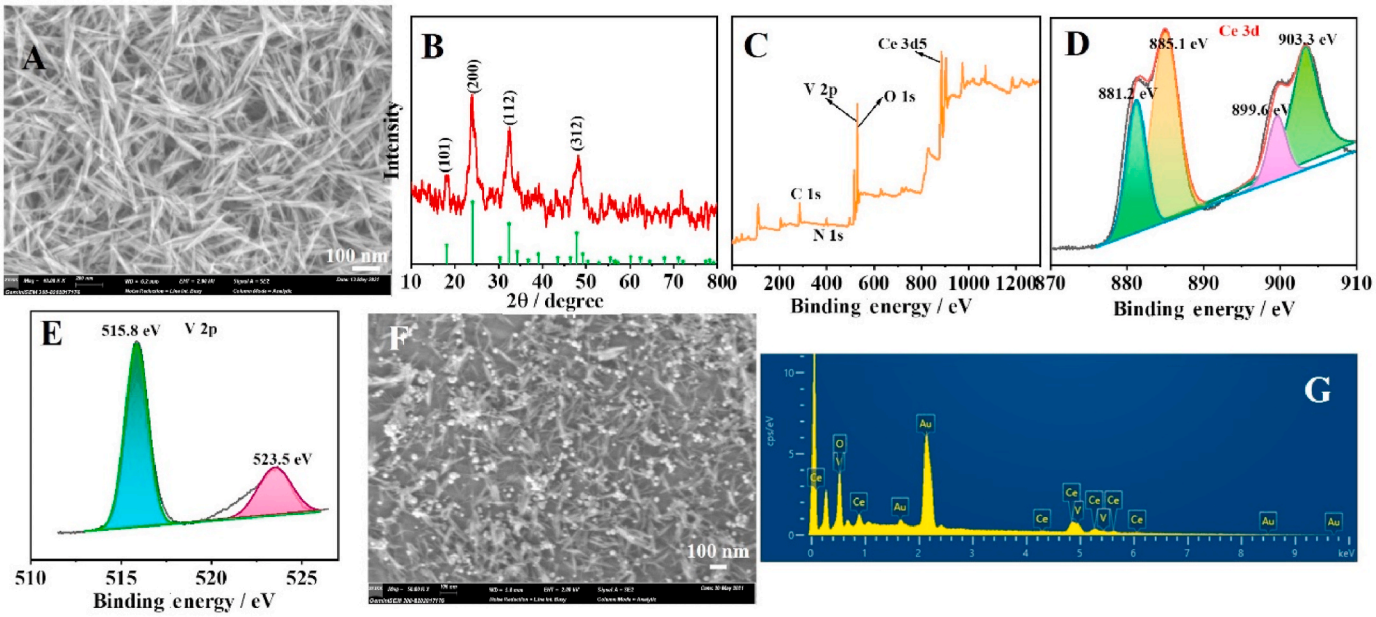


**Fig. 1.** (A) SEM and (B) XRD pattern of $CeVO_4$ nanorods. (C) XPS survey of $CeVO_4$ nanorods. High-resolution XPS spectra of Ce 3d (D) and V 2p (E). (F) SEM and (G) EDX spectrum of $CeVO_4$/Au.

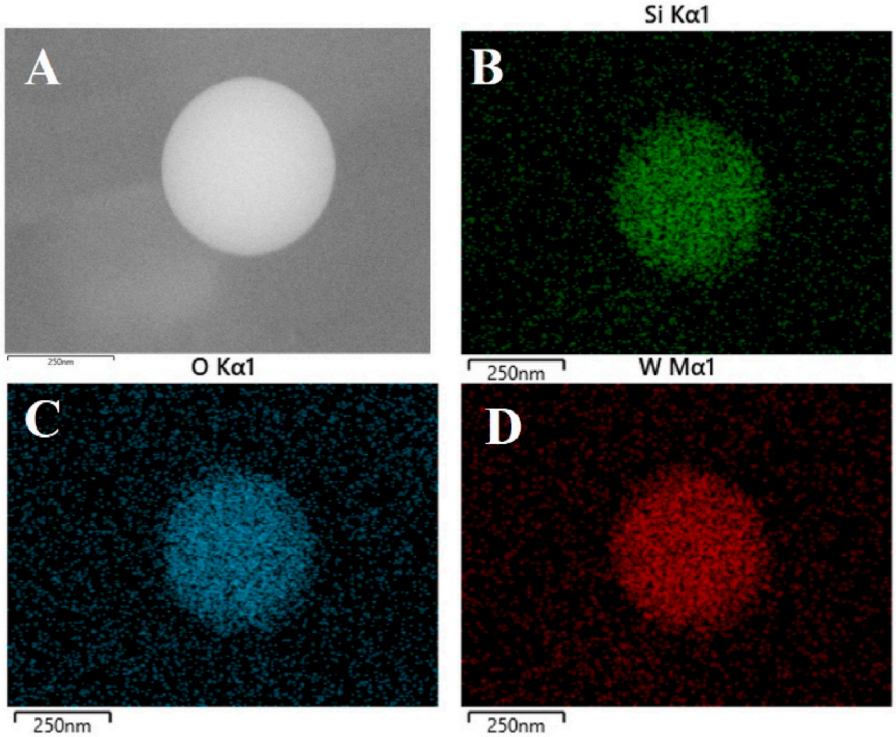


**Fig. 2.** (A) SEM of W-POM@$SiO_2$. Scanning elemental mapping of W-POM@$SiO_2$ showing distribution of Si (B), O (C) and W (D).

resulted from the excellent catalytic effect of $CeVO_4$/Au on the electro-oxidation of $H_2O_2$ to generate superoxide anion $O_2^{\bullet-}$ (eq. (1)), when the potential stepped from −0.6 V to +0.6 V, during which the luminol loaded on $CeVO_4$/Au deprotonated and was oxidized to generate intermediate oxidation state of luminol ($Lu^{-\bullet}$) (eq. (2)). In addition, the deprotonated luminol ($Lu^-$) could be directly oxidized by $O_2^{\bullet-}$ to form $Lu^{-\bullet}$ (eq. (3)). Subsequently, the reaction of $Lu^{-\bullet}$ with strong oxidant $O_2^{\bullet-}$ occurred to form the excited state of 3-aminophthalate ($3\text{-}AP^{2-*}$) for ECL emission around 435 nm (Fig. S2, curve a) (eqs. (4) and (5)).

After W-POM@$SiO_2$ was coated on ITO/Lu-$CeVO_4$/Au, the ECL signal remarkably decreased in contrast to the ECL intensity of ITO/Lu-$CeVO_4$/Au (Fig. 3A, curve c), conforming the quenching effect of W-POM on the ECL emission of Lu-$CeVO_4$/Au/$H_2O_2$ system due to the ROS-scavenging activity of W-POM (eq. (6)) [22,23]. Besides, the absorbance of W-POM was in the range of 530–800 nm (Fig. S2, curve b), which was far from the ECL wavelength, and excluded the energy transfer between excited $3\text{-}AP^{2-*}$ and W-POM. Thus the detailed ECL process could be described as follows:

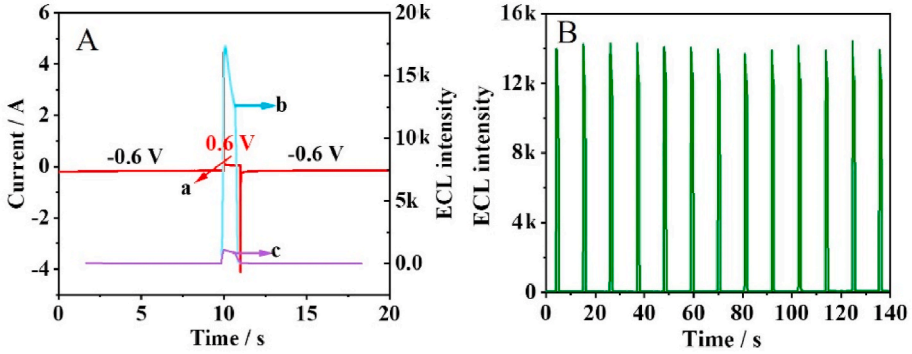


**Fig. 3.** (A) Current-time curve of ITO/Lu-$CeVO_4$/Au (a), and ECL-time curves of ITO/Lu-$CeVO_4$/Au (b) and ITO/Lu-$CeVO_4$/Au/W-POM@$SiO_2$ (c). (B) ECL signals of ITO/Lu-$CeVO_4$/Au under continuous potential step between −0.6 V and 0.6 V in 8 mM $H_2O_2$ (pH 8.0).

$$H_2O - \cdot e^- \xrightarrow{CeVO_4/Au} O_2^{\cdot -} + H_2O \quad (1)$$

$$Lu - H^+ \rightarrow Lu^- \xrightarrow{-e^-} Lu^{\cdot} \quad (2)$$

or

$$O_2^{\bullet -} + Lu^- \rightarrow Lu^{-\bullet} + HO_2^- \quad (3)$$

$$Lu^{-\bullet} + O_2^{\bullet -} \rightarrow 3\text{-}AP^{2-*} + N_2 \quad (4)$$

$$3\text{-}AP^{2-*} \rightarrow 3\text{-}AP^{2-} + h\nu \quad (5)$$

$$W^{5+} + O_2^{\bullet -} \rightarrow W^{6+} + H_2O \quad (6)$$

### 3.3. Characterizations of ECL immunosensor

Electrochemical impedance spectroscopy (EIS) was employed to confirm the successful fabrication of the developed immunosensor and the sandwich-typed immunoreactions on the immunosensor. The semicircle diameter was equal to the electron transfer resistance ($R_{et}$) at the electrode interface using $Fe(CN)_6^{3-/4-}$ as a couple of redox probes. After Lu-$CeVO_4$/Au was cast on ITO surface, the $R_{et}$ value greatly decrease due to the high conductivity of $CeVO_4$/Au (Fig. 4A, curves a and b). The immobilization of $Ab_1$ and then BSA resulted in the continuous increase of $R_{et}$ due to the presence of non-electric-conducted protein molecules (Fig. 4A, curves c and d). After NSE and $Ab_2$-W-POM@$SiO_2$ were conjugated to immunosensor surface via the sandwich-typed immunoreactions, the $R_{et}$ value further increased (Fig. 4A, curves e and f). Moreover, the ECL response also successively decreased upon the assembly of these proteins due to the increasing $R_{et}$ (Fig. 4B, curves b-d), and lastly showed the quenching of W-POM on the ECL emission of Lu-$CeVO_4$/Au/$H_2O_2$ system (Fig. 4B, curve e). More interestingly, all of the ECL emission at different modified electrodes showed good stability. These results demonstrated the feasibility of the proposed quenching strategy for ECL immunoassay of protein.

### 3.4. Condition optimization for ECL

The ECL signal of Lu-$CeVO_4$/Au/$H_2O_2$ system depended on the pH value of detection solution, which trended to the maximum intensity at

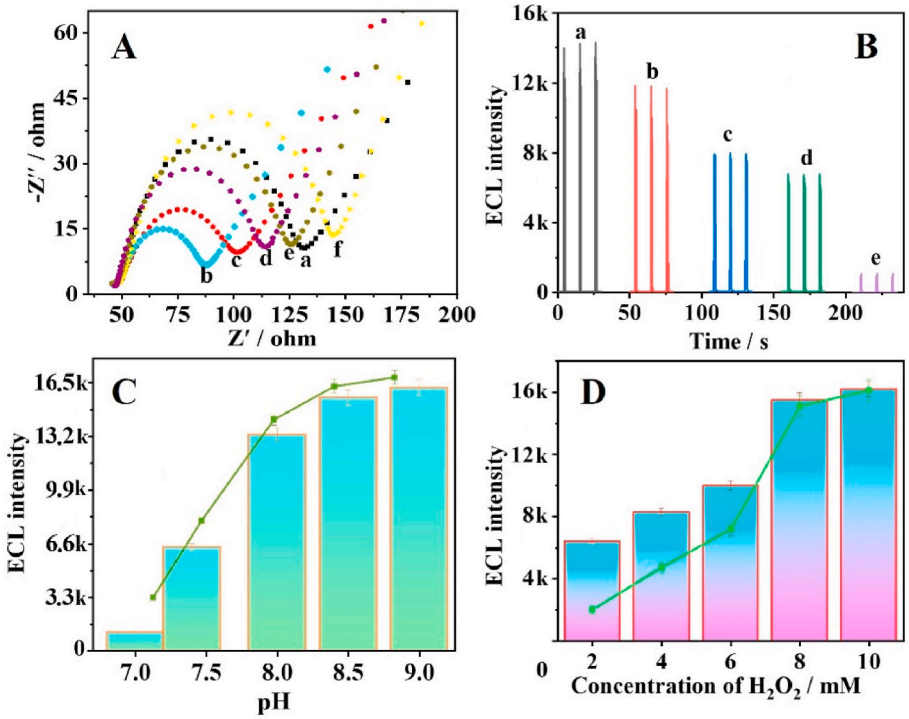


**Fig. 4.** (A) EIS of ITO (a), ITO/Lu-$CeVO_4$/Au (b), ITO/Lu-$CeVO_4$/Au/$Ab_1$ (c), ITO/Lu-$CeVO_4$/Au/$Ab_1$/BSA (d), $CeVO_4$/Au/$Ab_1$/BSA/NSE (e) and ITO/Lu-$CeVO_4$/Au/$Ab_1$/BSA/NSE/$Ab_2$-W-POM@$SiO_2$ (f) in 0.1 M $KNO_3$ containing 2.5 mM $Fe(CN)_6^{3-/4-}$. (B) ECL responses of ITO/Lu-$CeVO_4$/Au (a), ITO/Lu-$CeVO_4$/Au/$Ab_1$ (b), ITO/Lu-$CeVO_4$/Au/$Ab_1$/BSA (c), $CeVO_4$/Au/$Ab_1$/BSA/NSE (d) and ITO/Lu-$CeVO_4$/Au/$Ab_1$/BSA/NSE/$Ab_2$-W-POM@$SiO_2$ (e) in 8 mM $H_2O_2$ (pH 8.0). Effects of pH (C) and $H_2O_2$ concentration (D) on ECL intensity of ITO/Lu-$CeVO_4$/Au.

pH 8.0 (Fig. 4C). Therefore, pH 8.0 PBS was used throughout the sample analysis. The concentration of coreactant $H_2O_2$ was another important factor to affect the ECL emission. With the increasing $H_2O_2$ concentration, the ECL signal increased and reached the maximum value at 8 mM $H_2O_2$ (Fig. 4D), which was chosen as the optimized coreactant concentration for biomarker detection.

### 3.5. ECL immunoassay of NSE

Under the optimal detection conditions, the developed immunosensor was used for ECL immunoassay of NSE. With the increasing NSE concentration, the ECL intensity decreased after sandwich-typed immunoreactions (Fig. 5A, and inset in Fig. 5B). The plot of ECL intensity ($I$) vs the logarithm of NSE concentration (lg $c$) showed a linear relationship in the range from 0.5 pg/mL to 18 ng/mL (Fig. 5B). The linear regression equation was given as $I = -1078 \lg c$ (ng/mL) + 2641 with a $R^2$ value of 0.9913. The calculated detection limit at 3 σ was estimated to be 0.19 pg/mL. Benefiting from the advances of the proposed quenching strategy, the immunosensor performed a better analytical performance compared with other sensors (Table S1).

### 3.6. Stability, specificity and reproducibility of the immunosensor

Operation stability of the developed immunosensor was estimated by recording the ECL response in 8 mM $H_2O_2$ (pH 8.0) upon potential steps between −0.6 V and 0.6 V for 10 times at 2.00 ng/mL NSE (Fig. 5C), which gave a relative standard deviation (RSD) of 4.2%, indicating a good operation stability of the immunosensor. The selectivity of the immunosensor was assessed using 2.0 ng/mL NSE, and 100 ng/mL CEA, AFP, BSA and glucose as interferents. All of the interferents did not affect the ECL emission of the immunosensor for NSA, and their presence did also not interfere with the immunoassay of NSA (Fig. 5C), highlighting the good selectivity of the proposed method. The reproducibility of the proposed immunosensors was assessed by operating the ECL immunoassay at 5.00 ng/mL NSE with seven independent immunosensors, which showed the RSD of 2.0% (Fig. S3), revealing the satisfying reproducibility.

### 3.7. Application of the ECL immunoassay method

To assess the potential applicability of the ECL immunoassay method for NSE, the immunoassay was performed by spiking NSE solution at different concentrations in human serum samples. The recovery along with corresponding RSD values was listed in Table 1, which showed that the recovery was in the range of 98.5–113%, and the RSD values were less than 3.6%. These result were acceptable, and thereby demonstrated the good reliability and practicality of this method for real sample analysis.

## 4. Conclusion

A quenching-typed ECL immunosensing method has been proposed by using W-POM@$SiO_2$ to label the secondary antibody, which can efficiently quench the ECL emission of Lu-$CeVO_4$/Au/$H_2O_2$ system by the ROS-scavenging activity of W-POM to consume the co-reactant intermediate $O_2^{\bullet -}$. The immunosensor can be conveniently prepared by co-immobilizing capture antibody and Lu-$CeVO_4$/Au on ITO. The excellent catalytic effect of $CeVO_4$/Au leads to strong ECL emission of luminol in the presence of $H_2O_2$, thus the proposed immunosensing method possesses high sensitivity with a detection limit of sub-pg/mL level. The

**Table 1**
Detection of NSE in human serum samples.

| Sample | Addition (ng $mL^{-1}$) | Found (ng $mL^{-1}$) | RSD (%, $n$ = 11) | Recovery (%) |
|---|---|---|---|---|
| 1 | 15.0 | 14.9 | 1.4 | 99.3 |
| 2 | 5.00 | 5.13 | 2.7 | 103 |
| 3 | 0.500 | 0.569 | 3.6 | 114 |
| 4 | 0.00200 | 0.00197 | 2.1 | 98.5 |

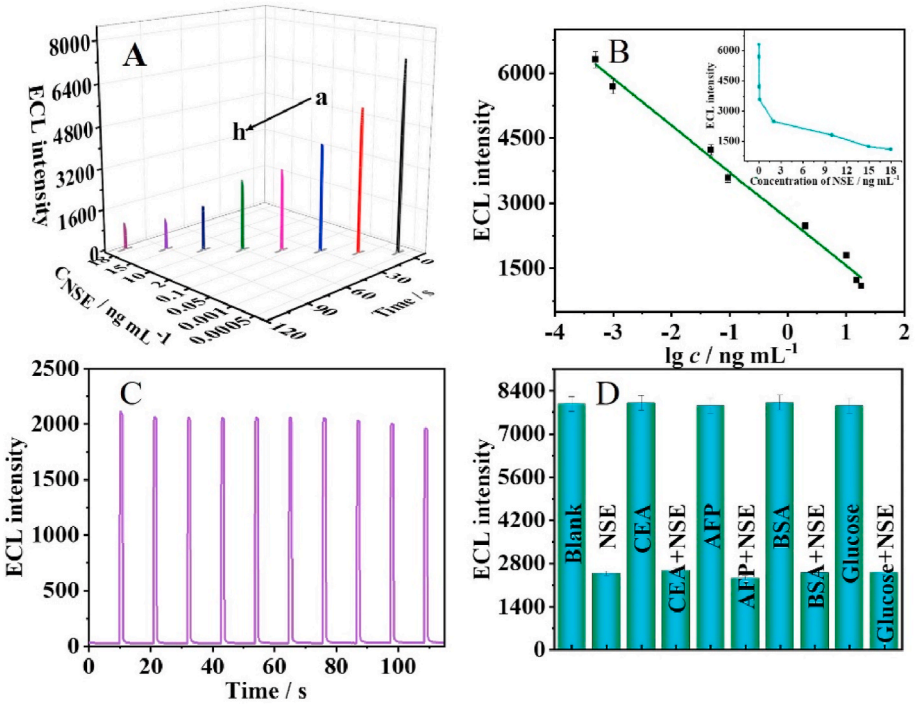


**Fig. 5.** (A) ECL responses of immunosensor to NSE at 0.0005, 0.001, 0.05, 0.1, 2.0, 10, 15 and 18 ng/mL (a to h). (B) Calibration curve. (C) Stability of ECL emission under continuous potential step for 10 cycles in PBS (pH 8.0) containing 8 mM $H_2O_2$ for detection of 5 ng/mL NSE. (D) Selectivity of the immunosensor against 100 ng/mL CEA, AFP, BSA, glucose, and 2.00 ng/mL NSE. Error bars: RSD ($n$ = 3).

stable ECL emission of Lu-$CeVO_4$/Au/$H_2O_2$ system assures the excellent performance of immunosensor with good operation stability and satisfying reproducibility. More importantly, this proposed quenching strategy does not influence the electron transfer of luminophores with electrode, and can be applied to construct different sandwich-typed immunoassay methods for various protein biomarkers.

## CRediT authorship contribution statement

**Yu Du:** Conceptualization, Data curation, Writing – original draft. **Siqi Yu:** Formal analysis. **Huangxian Ju:** Funding acquisition, Project administration, Writing – review & editing.

## Declaration of competing interest

The authors declare that they have no known competing financial interests or personal relationships that could have appeared to influence the work reported in this paper.

## Acknowledgments

This work was financially supported by the National Natural Science Foundation of China (21827812, 21890741).

## Appendix A. Supplementary data

Supplementary data to this article can be found online at https://doi.org/10.1016/j.aca.2022.339883.

## References

[1] Y. Sun, Y. Zhang, H. Zhang, M. Liu, Y. Liu, Integrating highly efficient recognition and signal transition of g-$C_3N_4$ embellished $Ti_3C_2$ MXene hybrid nanosheets for electrogenerated chemiluminescence analysis of protein kinase activity, Anal. Chem. 92 (2020) 10668–10676.
[2] M.F. Sun, J.L. Liu, Y.Q. Chai, J. Zhang, Y. Tang, R. Yuan, Three-dimensional cadmium telluride quantum dots–DNA nanoreticulation as a highly efficient electrochemiluminescent emitter for ultrasensitive detection of microRNA from cancer cells, Anal. Chem. 91 (2019) 7765–7773.
[3] Z.Y. Liu, W.J. Qi, G.B. Xu, Recent advances in electrochemiluminescence, Chem. Soc. Rev. 44 (2015) 3117–3142.
[4] H. Lu, J. Pan, Y. Wang, S.Y. Ji, Z. Wei, X. Luo, J.J. Xu, H.Y. Chen, Electrochemiluminescence energy resonance transfer system between RuSi nanoparticles and hollow Au nanocages for nucleic acid detection, Anal. Chem. 90 (2018) 10434–10441.
[5] Z. Huang, Z. Li, L. Xu, C. Wei, C. Zhu, H. Deng, H. Peng, X. Xia, W. Chen, Mechanistic insight into a novel ultrasensitive nicotine assay base on high-efficiency quenching of gold nanocluster cathodic electrochemiluminescence, Anal. Chem. 92 (2020) 11438–11443.
[6] M. Xia, F. Zhou, X. Feng, J. Sun, L. Wang, N. Li, X. Wang, G. Wang, A DNAzyme-based dual-stimuli responsive electrochemiluminescence resonance energy transfer platform for ultrasensitive anatoxin-a detection, Anal. Chem. 93 (2021) 11284–11290.
[7] W. Cao, J.P. Fe rrance, J. Demas, J.P. Landers, Quenching of the electrochemiluminescence of tris(2,2'-bipyridine)ruthenium(II) by ferrocene and its potential application to quantitative DNA detection, J. Am. Chem. Soc. 128 (2006) 7572–7578.
[8] J.L. Liu, R. Yang, Y.Q. Chai, R. Yuan, Versatile luminol/dissolved oxygen/Fe@$Fe_2O_3$ nanowire ternary electrochemiluminescence system combined with highly efficient strand displacement amplification for ultrasensitive microRNA detection, Anal. Chem. 93 (2021) 13334–13341.
[9] S. Deng, H. Ju, Electrogenerated chemiluminescence of nanomaterials for bioanalysis, Analyst 138 (2013) 43–61.
[10] J. Sun, H. Sun, Z. Liang, Nanomaterials in electrochemiluminescence sensors, Chemelectrochem 4 (2017) 1651–1662.
[11] Y. Du, J. Xue, X. Sun, D. Wu, X. Liu, H. Ju, L. Yang, Q. Wei, Oxygen vacancy-enhanced electrochemiluminescence sensing strategy using luminol thermally encapsulated in apoferritin as a transducer for biomarker immunoassay, Anal. Chem. 92 (2020) 8472–8479.
[12] L. Yang, J. Xue, Y. Jia, Y. Zhang, D. Wu, H. Ma, Q. Wei, H. Ju, Construction of well-ordered electrochemiluminescence sensing interface using peptide-based specific antibody immobilizer and N-(aminobutyl)-N-(ethylisoluminol) functionalized ferritin as signal indicator for procalcitonin analysis, Biosens. Bioelectron. 142 (2019), 111562.
[13] P. Ju, Y. Yu, M. Wang, Y. Zhao, D. Zhang, C. Sun, X. Han, Synthesis of EDTA-assisted $CeVO_4$ nanorods as robust peroxidase mimics towards colorimetric detection of $H_2O_2$, J. Mater. Chem. B. 4 (2016) 6316–6325.
[14] M. Chang, M. Wang, Y. Chen, M. Shu, Y. Zhao, B. Ding, Z. Hou, J. Lin, Self-assembled $CeVO_4$/Ag nanohybrid as photoconversion agents with enhanced solar-driven photocatalysis and NIR-responsive photothermal/photodynamic synergistic therapy performance, Nanoscale 11 (2019) 10129–10136.
[15] L. Yang, Y. Jia, D. Wu, Y. Zhang, H. Ju, Y. Du, H. Ma, Q. Wei, Synthesis and application of $CeO_2$/$SnS_2$ heterostructures as a highly efficient coreaction accelerator in the luminol-dissolved $O_2$ system for ultrasensitive biomarkers immunoassay, Anal. Chem. 91 (2019) 14066–14073.
[16] A. Proust, R. Thouvenot, P. Gouzerh, Functionalization of polyoxometalates: towards advanced applications in catalysis and materials science, Chem. Commun. (2008) 1837–1852.
[17] Y.F. Song, R. Tsunashima, Recent advances on polyoxometalate-based molecular and composite materials, Chem. Soc. Rev. 41 (2012) 7384–7402.
[18] A. Bijelic, M. Aureliano, A. Rompel, The antibacterial activity of polyoxometalates: structures, antibiotic effects and future perspectives, Chem. Commun. 54 (2018) 1153–1169.
[19] A. Bijelic, A. Rompel, Ten good reasons for the use of the tellurium-centered anderson-evans polyoxotungstate in protein crystallography, Acc. Chem. Res. 50 (2017) 1441–1448.
[20] J. Zhou, W. Zhao, Z. Miao, J. Wang, Y. Ma, H. Wu, T. Sun, H. Qian, Z. Zha, Folin–ciocalteu assay inspired polyoxometalate nanoclusters as a renal clearable agent for non-inflammatory photothermal cancer therapy, ACS Nano 14 (2020) 2126–2136.
[21] H. Tawarayama, F. Utsuno, H. Inoue, H. Hosono, H. Kawazoe, Coloration and decoloration of tungsten phosphate glasses by heat treatments at the temperature far below Tg under a controlled ambient, Chem. Mater. 18 (2006) 2810–2816.
[22] P. Liu, Y. Wang, L. An, Q. Tian, J. Lin, S. Yang, Ultrasmall $WO_3$–X@γ-poly-L-glutamic acid nanoparticles as a photoacoustic imaging and effective photothermal-enhanced chemodynamic therapy agent for cancer, ACS Appl. Mater. Interfaces 10 (2018) 38833–38844.
[23] B. Geng, X. Yang, P. Li, W. Shi, D. Pan, L. Shen, W-doped $TiO_2$ nanorods for multimode tumor eradication in osteosarcoma models under single ultrasound irradiation, ACS Appl. Mater. Interfaces 13 (2021) 45325–45334.
[24] E. Ma, P. Wang, Q. Yang, H. Yu, F. Pei, Y. Zheng, Q. Liu, Y. Dong, Y. Li, Electrochemical immunosensors for sensitive detection of neuron-specific enolase based on small-size trimetallic Au@Pd^Pt nanocubes functionalized on ultrathin $MnO_2$ nanosheets as signal labels, ACS Biomater. Sci. Eng. 6 (2020) 1418–1427.
[25] N. Singh, S.K. NaveenKumar, M. Geethika, G. Mugesh, A cerium vanadate nanozyme with specific superoxide dismutase activity regulates mitochondrial function and ATP synthesis in neuronal cells, Angew. Chem. Int. Ed. 60 (2021) 3121–3130.